metals

Article

Analysis of Composition, Properties, and Usage Efficiency of Different Commercial Salt Fluxes for Aluminum Alloy Refining

Boris Kulikov [1], Evgeniy Partyko [2], Aleksandr Kosovich [2,*], Pavel Yuryev [3], Yulbarskhon Mansurov [4,5], Nikita Stepanenko [2], Yuriy Baykovskiy [2], Dmitry Bozhko [3], Alexander Durnopyanov [2], Nikolay Dombrovskiy [3] and Maxim Baranov [2]

[1] Laboratory of X-Ray Research and Analysis Methods, Siberian Federal University, 660041 Krasnoyarsk, Russia
[2] School of Non-Ferrous Metals, Siberian Federal University, 660041 Krasnoyarsk, Russia
[3] Laboratory of Low-Carbon Metallurgy and Energy, Siberian Federal University, 660041 Krasnoyarsk, Russia
[4] Department of Wagons and Wagon Economy, Tashkent State Transport University, Tashkent 100067, Uzbekistan
[5] College of Chemical Engineering, Huanggang Normal University, Huanggang 438000, China
* Correspondence: akosovich@sfu-kras.ru

Abstract: One of the key problems in the billet and shaped casting of aluminum alloys is the presence of various undesirable inclusions and impurities in the melt, which can serve as stress concentrators in the finished product, as well as dissolved hydrogen, which contributes to the formation of porosity. The interaction of aluminum with other gases produced by the combustion of fuel particles, oil, and paint materials brought into the furnace together with charge and scrap increases the amount of nitrides, oxides, carbides, and sulfides in the melt. Flux treatment is widely used as protection of aluminum alloys from oxidation and removal of impurities. The present paper reports the data of a comparative analysis of five widely used flux compositions based on sodium, potassium, and magnesium chlorides. The study covers the following aspects: chemical composition, moisture content, melting temperature and melting range, particle size distribution, and refining ability as measured by the change in Na, Ca, and H_2 content after melt treatment.

Keywords: aluminum alloy; melt treatment; salt flux; recycling; refining; degassing; hydrogen content; impurities; chloride; fluoride; crystalline hydrate

check for updates

Academic Editor: Mark E. Schlesinger

Received: 18 March 2025
Revised: 1 April 2025
Accepted: 14 April 2025
Published: 16 April 2025

Citation: Kulikov, B.; Partyko, E.; Kosovich, A.; Yuryev, P.; Mansurov, Y.; Stepanenko, N.; Baykovskiy, Y.; Bozhko, D.; Durnopyanov, A.; Dombrovskiy, N.; et al. Analysis of Composition, Properties, and Usage Efficiency of Different Commercial Salt Fluxes for Aluminum Alloy Refining. *Metals* **2025**, *15*, 448. https://doi.org/10.3390/met15040448

Copyright: © 2025 by the authors. Licensee MDPI, Basel, Switzerland. This article is an open access article distributed under the terms and conditions of the Creative Commons Attribution (CC BY) license (https://creativecommons.org/licenses/by/4.0/).

1. Introduction

In terms of the total volume of castings produced in the last decade, three classes of materials—cast iron; steel; and aluminum—have been dominant. At the same time, the current opinions of industry experts suggest a significant growth in the production of aluminum and cast parts from it, with a decrease in the production of cast iron in almost equal proportion, as well as a slowdown in the growth rate of the crude steel market. One of the main reasons for such changes can be considered to be the effort to achieve carbon neutrality, since the international community is concerned about the problem of climate change and considers the possibility of radical reduction of greenhouse gas emissions as the main mechanism for its mitigation [1–4]. This, in turn, stimulates the transition to low-emission materials both at the production stage and during the life cycle.

In addition, great attention is paid to reducing the weight of metal components while maintaining their performance properties, which increases consumer demand for cast parts and deformable semi-finished products made of aluminum alloys for the automotive [5] and aerospace [6] industries (where it directly affects fuel consumption and controllability),

building and construction [7], and other industries [2]. The main consumer and, consequently, the source of scrap in this context is the automotive industry, which additionally contributes to the increase in the extraction and involvement of rare and rare-earth metals used for direct addition to the liquid melt at the production stage [8] or the development of electronic components, electric engines, and batteries [9,10]. This is directly related to the development of new hybrid and full-electric-powered transportation, as well as related research on the extraction and reuse of rare and rare earth metals in the end-of-life phase [11,12].

The above trends contribute to the improvement and emergence of new solutions for the production of high-purity raw aluminum and commercial alloys [13,14], scrap recycling, and the production of secondary alloy products [15,16]. Aluminum scrap recycling technologies [2,17,18] are being developed to a greater extent due to the significant economic and environmental benefits, as these solutions can reduce harmful emissions and energy consumption by up to 90–95% compared to primary aluminum production. Today, about 35% of aluminum production is related to recycling and the production of secondary alloy products. It is expected that by 2050 the amount of secondary aluminum will already be about 50% of total production, as shown in Figure 1. According to preliminary estimates, this trend, together with the increasing share of aluminum components in transport, will prevent tens of millions of tons of CO_2 emissions annually by 2030 [3,19].

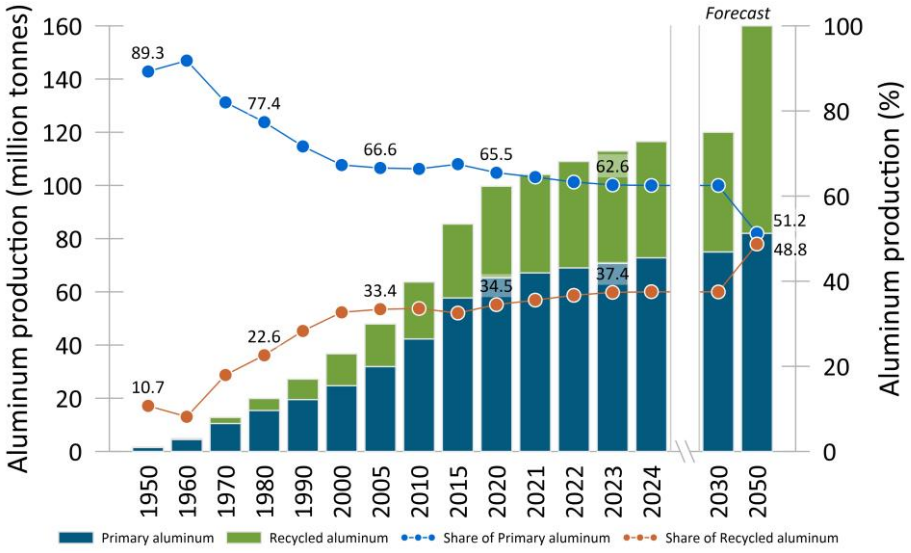

Figure 1. Global aluminum production. Data collected from [1–4].

It is important to note that in aluminum scrap recycling there are two flows with different characteristics: first, new scrap (also known as post-production, pre-consumer), which is generated during the production process and often has a strictly defined affiliation to a particular alloy grade; second, old scrap (also known as post-consumer, end-of-life), which requires careful sorting and preparation before remelting. A generalized scheme of commercial and secondary alloy smelting, manufacturing, and use of products with separation of scrap flows is presented in Figure 2. According to collected data and statistical forecasts [2,3], the situation with respect to these flows is changing. Around 1990, the share of each flow was almost equal, but over time there has been a trend towards the predominance of old scrap in global recycled aluminum: in 2020, the share of post-consumer scrap was about 60%, while post-production scrap was 40%. By 2030, the distribution of shares will have an even wider gap: 64% post-consumer and 36% post-production. By 2050, the ratio will be 70/30. However, the continuation of the forecast trend depends on the interaction of such factors as the increased use of aluminum in metal-intensive

assemblies, the reliability of scrap collection and supply chains, the development of scrap sorting and quality control technologies, the improvement of melt purification methods, and the competitiveness of secondary alloy products.

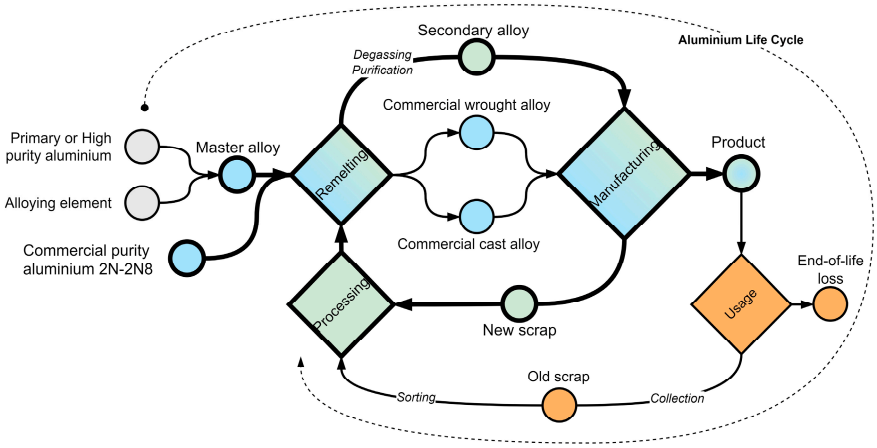

Figure 2. Aluminum life cycle and common product manufacturing scenarios. The technological process realized in this work is shown by bold lines.

Nevertheless, regardless of the initial metal raw material (primary aluminum, commercial grade, or secondary alloys), for the consumer, the performance properties of products are important, characterizing the resistance of the material to the occurrence and growth of micro- and macro-cracks. Pores and non-metallic inclusions are stress concentrators that can intensify cracking in aluminum products [20]. Accordingly, the lower the grade of the feed material and/or the higher the percentage of scrap involved, the more attention should be paid to degassing and refining operations [21–23], as well as protection of the aluminum melt from interaction with the plant atmosphere [24–26]. The industry uses a number of methods of melt refining and degassing to remove contaminants, as shown in Table 1, but the choice of one or another method is usually justified not by efficiency but by the technical and resource conditions of a particular casting shop (plant).

Table 1. Examples of undesirable impurities specific to aluminum alloys.

Impurities	Origins	Issues	Countermeasures	Ref.
H_2	Interaction of melt with atmosphere, combustion products; moisture of unprepared charge materials, lining, tools; turbulent flow of melt	Gas porosity; reduction of mechanical properties	Fluxing; thermal and temporal treatment; ultrasonic treatment; flotation (degassing with inert or active gases); vacuuming; electromagnetic treatment	[27–34]
Na Ca	Low-grade charge; impurities in master alloys; interaction of melt with lining	Formation of undesirable inclusions; reduction of casting properties, machinability; increased tendency to cracking	Fluxing; flotation (active gas purging)	[35–40]
Fe	Low-grade charge; impurities in master alloys; tool erosion	Reduction of casting and mechanical properties	Sedimentation; electric pulse treatment; compensation of influence by additional alloying; ultrasonic treatment	[41–45]
Al_2O_3, MgO, $MgAl_2O_4$, AlN, SiO_2	Interaction of melt with atmosphere, lining	Reduction of mechanical properties, corrosion resistance, machinability	Fluxing; filtration; flotation (active gas purging)	[46–50]

Many of the purification methods can be successfully combined, in which case the application of a complex solution depends on the features of the technological sequence, type of products, productivity, etc. A widespread solution for aluminum alloys is salt

flux treatment (fluxing), often in combination with the use of rotary degassers [28,33,51]. Commercial solid salt fluxes in powder or granular form are compositions consisting of chlorides such as NaCl, KCl, $MgCl_2$, $AlCl_3$, and fluorides such as AlF_3, NaF, CaF_2, MgF_2, Na_2SiF_6, Na_3AlF_6, and K_2SiF_6 [52–55]. Depending on the predominant base component, fluxes can be divided into three functional groups: covering fluxes, protecting liquid metal from oxidation and hydrogenation; dross fluxes, reducing the aluminum content in slag and facilitating its removal; and refining fluxes, promoting melt degassing, transfer of inclusions, and undesirable elements into slag. Studies have been published on the development of more universal compositions based on the NaCl–KCl system with additives of various fluorides [56], as well as having as a base a combination of KCl, Na_2CO_3, Na_2SO_4, K_2CO_3, $NaNO_3$, and Na_3AlF_6 [57]. Fluxes containing K_2TiF_6 and KBF_4 are of particular interest: the processing of Al-Si alloys with this kind of composition makes it possible to combine purification and grain refining operations [58,59].

Based on the above, it is possible to assume the existence of numerous publications on the topic of salt fluxes. However, most of them focus on the properties of classical mixtures with functional additives (e.g., KCl–NaCl system + fluoride). Whereas only a small part of publications is devoted to the verification of melt cleaning efficiency and to the analysis of flux composition used in industrial rather than laboratory scale. The aim of the present research is a comprehensive analysis of the relationships between composition, moisture content, melting temperature, particle size distribution, and their combined effect on the refining ability in relation to the changes of Na, Ca, and H_2 content in aluminum melt. Particular attention is paid to the effect of solid fluxes on melt purity in experiments approximating industrial ingot casting. The latter aspect is particularly important and contributes to a general understanding of the behavior of the different flux components, which is often unknown to operators.

2. Materials and Methods

In the present study, 5 commercial solid salt fluxes are investigated, which are widely used in industrial practice at foundries in Russia, China, and the Commonwealth of Independent States. The identity of the flux manufacturers is not given to avoid any type of commercial influence and reputational implications. Since the salt fluxes investigated in this work are commercially available, in the text they are assigned the conventional designations "SF*n*", where *n* is a sequence number from 1 to 5.

X-ray phase analysis of fluxes was performed on an automated diffractometer, XRD-7000 (Shimadzu, Kyoto, Japan), in Cu-Kα radiation. X-ray diffractograms were taken on powders in the range of angles 2θ from 5° to 70° with a step of 0.03° and a scanning speed of 1.5 deg/min. A finely powdered sample of each salt flux was manually pressed into a standard quartz glass cuvette. Phase identification was performed automatically by using the database of X-ray phase standards of minerals supplied with the instrument according to the multireflex method of "corundum numbers". This method is realized through the ratio of maximum intensities to the reference phase, which is corundum (α-Al_2O_3). Refinement of the automatic identification was performed, taking into account the results of X-ray spectral analysis (XRD) obtained using a XRF-1800 wave spectrometer (Shimadzu, Kyoto, Japan) with an Rh anode.

Thermal analysis was performed on a synchronous analyzer SDT Q 600 (TA Instruments, New Castle, DE, USA). The analyzer allows simultaneously obtaining data on the sample weight change, rate of weight change, thermal effects in the system, and the composition of the released gas phase during heating of the sample. Thermograms were taken when fluxes were heated at a rate of 20 deg/min in an air atmosphere to a temperature of 300–400 °C, with an air purge rate of 50 mL/min. Heating of fluxes to the melting point

was not carried out because of the risk of damage to the analyzer due to the high fluidity of fluxes. The sample weights were 20 mg.

The melting interval of fluxes was determined by the curve on the heating line of the salt flux from the beginning of liquid phase formation to complete melting [60]: during melting, the temperature rise slows down for some time, then the growth continues; therefore, the temperature of the beginning and end of the "kink" segment on the heating curve of the flux corresponds to the melting interval. A graphite crucible was placed on a stand in the induction furnace, in which a smaller porcelain crucible was placed with a sample of the flux under study (10 g); porcelain crucibles were previously calcined at 700 °C. A thermocouple (without a protective case), connected to a device to control the temperature change, was immersed in the flux sample to the same depth. After melting the flux, the furnace was switched off, the hot crucible with the molten flux sample was removed from the furnace and weighed after cooling, and the weight loss of the flux was calculated from the results of weighing. Additionally, the melting point of fluxes was calculated from melting diagrams of systems based on chlorides of alkali and alkaline-earth metals.

The particle size distribution of salt fluxes was determined with a vibrating sieve calibrator, providing sieve vibration with an amplitude of vibration of 0.1–1.0 mm and a frequency of 50 vibrations/s, using a set of sieves with a mesh size from 2.5 to 0.05 mm. After sieving, each part of the sample distributed into fractions was weighed separately to the nearest 0.01 g, and its fraction relative to the original weight of the whole sample was calculated.

Experiments to evaluate the effectiveness of different salt fluxes were performed in a scenario where a notional producer remelts a commercial purity feedstock, such as 2N5 or 2N7 [14], with the addition of alloying components to prepare a secondary alloy and then produce semi-finished products. The scenario of semi-finished product manufacturing was realized using the direct chill casting unit shown in Figure 3, which allows simulating industrial technological processes on a laboratory scale.

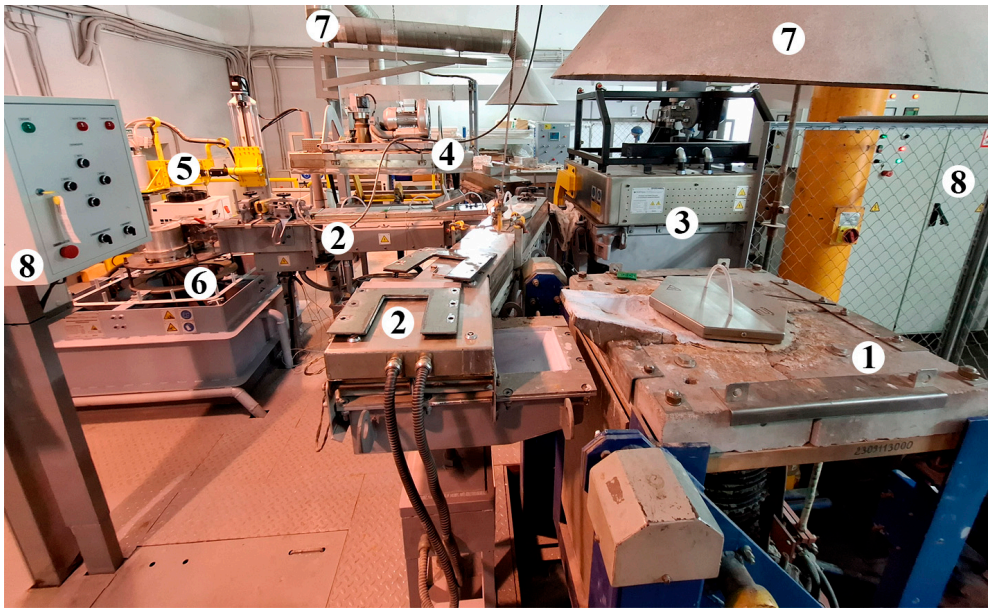

Figure 3. Semi-continuous ingot casting unit: 1—tilting melting induction furnace; 2—heated channel for molten metal flow; 3—holding furnace with an argon purging system and a magnetohydrodynamic stirring module; 4—melt filtration system; 5—ultrasonic processing module; 6—vertical direct chill casting machine; 7—exhaust ventilation of the working area; 8—control panel. The elements 3, 4, and 5 were not used in the actual study.

The refining ability of the studied salt fluxes, i.e., the efficiency of removal of sodium, calcium, and dissolved hydrogen from the melt, was evaluated as follows, as shown in Figure 4. First, aluminum ingots of commercial purity 2N7 (KrAZ, Krasnoyarsk, Russia) were melted. Second, a calculated amount of alloying components was added to the melt to bring the melt to the nominal chemical composition (Table 2). The mass of the finished alloy subjected to flux treatment was 40 kg in all experiments. Thirdly, the melt condition was monitored: temperature was measured, three samples were taken to determine the chemical composition and dissolved hydrogen content, and the content of impurities before fluxing was recorded. Fourthly, the melt was treated with flux with stirring according to the average consumption of 1.25 kg per 1 ton of metal. Fifthly, three samples were taken again, and the content of impurities was recorded after fluxing. This sequence was performed separately for each of the investigated salt fluxes.

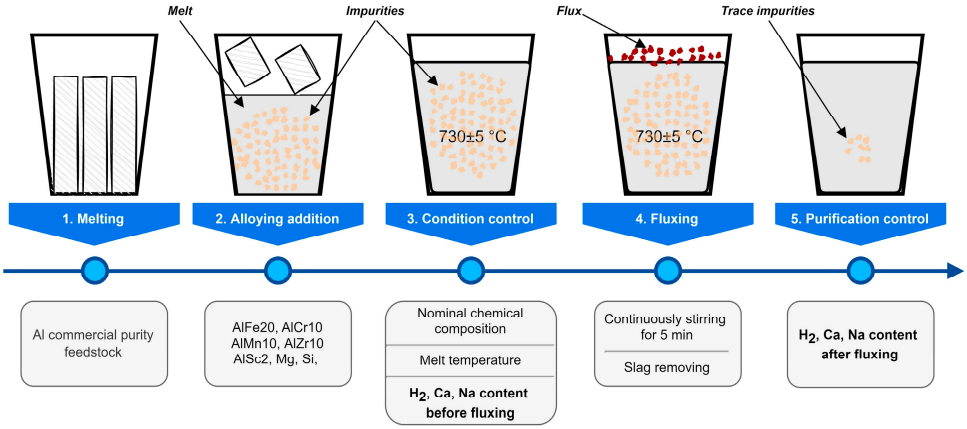

Figure 4. Flowchart of the experimental process with melt.

Table 2. Nominal alloy chemical composition (wt.%).

Mg	Mn	Fe	Cr	Zr	Si	Sc	Al
4.95 ± 0.5	0.6 ± 0.10	0.15 ± 0.02	0.15 ± 0.02	0.11 ± 0.04	0.11 ± 0.04	0.10 ± 0.02	Bal.

The chemical composition of the alloy was determined on a FOUNDRY-MASTER LAB optical emission spectrometer (Hitachi High-Tech Analytical Science, Abingdon, UK) with an optical system according to the Paschen-Runge scheme; for the taking and crystallization of these samples, we used a steel split cauldron with a copper base. The hydrogen concentration in the melt was determined with an ALU COMPACT II apparatus (FMA Mechatronic Solutions, Schaan, Liechtenstein) according to the "first bubble" method used as an express test [61]. The temperature of the liquid melt in the induction furnace was 730 ± 5 °C. The temperature was controlled by an IT-8 gauge (Relsib, Novosibirsk, Russia) with a connected thermocouple, TP 008 #21-ANXGX (Sputnik, Krasnoyarsk, Russia).

3. Results and Discussions

Fluxes for processing aluminum alloys should have a number of properties that determine their effectiveness: the melting point of the flux should be lower than the melt temperature; the density of liquid fluxes and slags based on them should be less than the density of the liquid metal; fluxes should wet non-metallic inclusions well; the hygroscopicity of fluxes should be as low as possible to prevent contamination of the melt with hydrogen; and exhaust fluxes and their components should be easily removed from the surface of the melt. The chemical composition of the flux can be selected to provide the desired density, viscosity, wettability, melting point, hygroscopicity, etc. Some of these

properties are described below with emphasis on how they affect the application of fluxes in simulated industrial environments.

3.1. Phase Composition

To obtain a more homogeneous assessment of the composition of each flux, XRD analysis was performed on three consecutive samples taken from the same batch of material. The samples were taken as quickly as possible after removal from the sealed bags to avoid the interaction of sample components with air moisture, since the hygroscopicity of individual components can affect the results. X-ray patterns of the studied salt fluxes are presented in Figure 5; the general characterization of the identified components is given in Table 3.

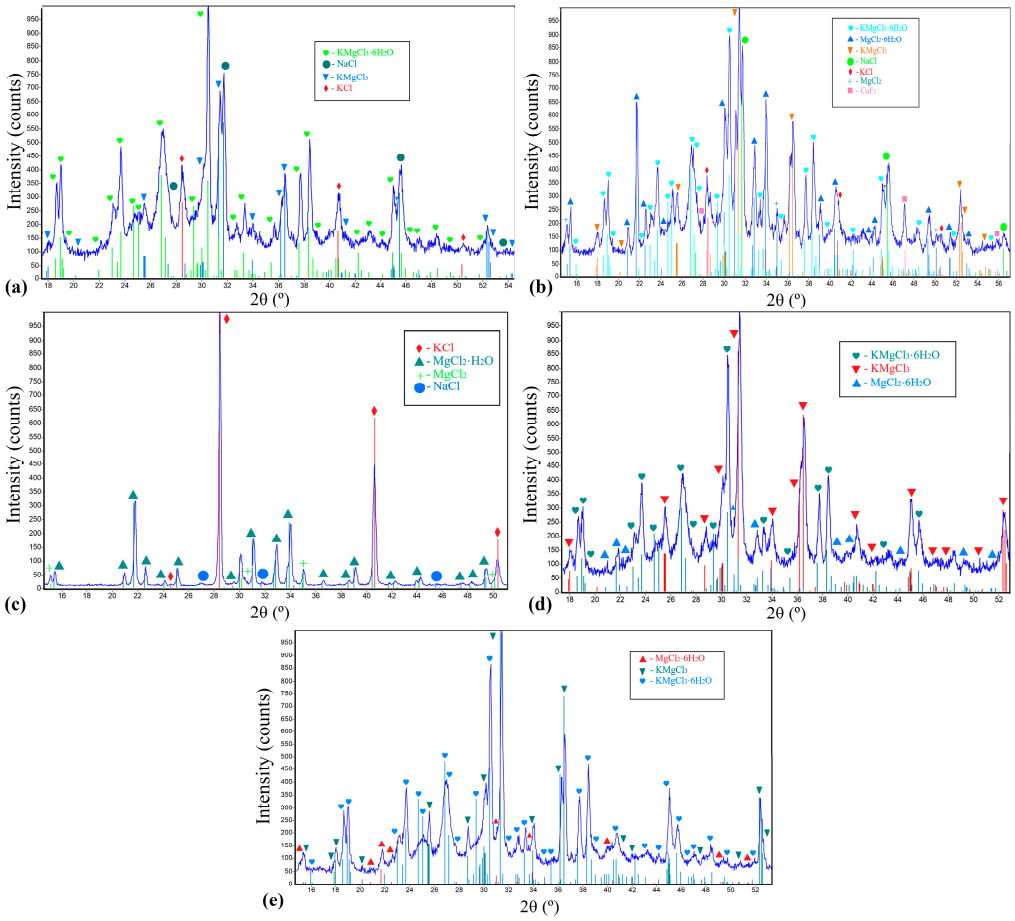

Figure 5. XRD patterns of the investigated salt fluxes: (**a**) SF1; (**b**) SF2; (**c**) SF3; (**d**) SF4; (**e**) SF5.

Sodium and potassium chlorides are among the basic fillers in flux compositions, but when used individually, they have negligible reactivity in the aluminum melt. Because of this, in most cases they are used as an equimolar mixture, forming a low-temperature eutectic. Mixtures based on the KCl–NaCl system are used as covering fluxes to protect the melt from oxidation and hydrogenation since they have high fluidity and can form a thin layer on the surface of the liquid metal [55,62]. To provide refining properties and more effective slag separation and melt purification, as well as to change the viscosity of the flux, NaF, KF, CaF_2, and Na_2SiF_6 are additionally introduced into the composition (up to 5 wt.%).

Table 3. Characterization of flux components. Data collected from [55,62–64].

Chemical Formula	Chemical Composition (wt.%)		Melting Point (°C)	Solid Density (g/cm^3)	Liquid Density (g/cm^3)	Comment
KCl	K	52.44	770	1.984	1.527	Hygroscopic salt. Increases fluidity. Acts as a covering component.
	Cl	47.56				
NaCl	Na	39.34	801	2.165	1.556	Increases fluidity. At high concentrations increases the melting point of the flux. Acts as a covering component.
	Cl	60.66				
$KMgCl_3$ ($KCl{\cdot}MgCl_2$)	K	23.21	485	2.260	1.650	Reduces flux melting point, increases viscosity. Acts as a refining component.
	Mg	14.29				
	Cl	62.50				
$KMgCl_3{\cdot}6H_2O$ ($KCl{\cdot}MgCl_2{\cdot}6H_2O$)	K	14.07	–	1.600	–	Hydrated potassium and magnesium chloride melts when heated and dissolves in its own crystallization moisture.
	Mg	8.750				
	Cl	38.28				
	H	4.350				
	O	34.55				
$MgCl_2$	Mg	25.53	714	2.320	1.680	Hygroscopic salt. Reduces flux melting point, increases fluidity. Acts as a refining component.
	Cl	74.47				
$MgCl_2{\cdot}6H_2O$	Mg	11.96	117	1.569	–	Hydrated magnesium chloride cracks when heated and emits water vapor and HCl.
	Cl	34.88				
	H	5.950				
	O	47.22				
CaF_2	Ca	51.33	1423	3.180	2.520	Increases wettability. Acts as a refining additive.
	F	48.67				

$MgCl_2$–KCl is another common base, more commonly used for refining fluxes. Although relatively expensive, such compositions have shown promise in the processing of Al–Mg alloys, where it is particularly important to prevent an increase in sodium content and reduce calcium. Solid salt fluxes with $MgCl_2$ are an environmentally acceptable alternative to chlorine gas purging, which is currently banned in many countries for health and safety reasons [52,57].

In contrast to KCl–NaCl and $MgCl_2$–KCl systems widely spread in the USA and Europe, halides in the form of crystalline hydrates ($KCl{\cdot}MgCl_2{\cdot}6H_2O$, $MgCl_2{\cdot}6H_2O$) are more often in the focus of research and application at the plants of Russia and the Commonwealth of Independent States. For example, dehydrated double chloride $KCl{\cdot}MgCl_2$ can act both as an independent refining flux and as the basis of a mixture with additives of NaCl, CaCl, and other components that impart covering properties [60,65,66]. However, the production of such fluxes involves technological aspects of the dehydration of crystalline hydrates, remelting of the mixture, and grinding of the obtained material, which affects the final cost of the product.

Based on the obtained XRD patterns (Figure 5) and known literature information on the functional properties of the salt components (Table 3), the diagram shown in Figure 6 was drawn up. On the diagram, the axes indicate the content (wt.%) of the main salt components; the colored areas correspond to the chemical composition of the studied fluxes. The faces of the background polygon reflect the functions of the mixture, the area of which is located between the corresponding axes of components. Thus, it is possible to carry out graphically a comparative analysis of investigated fluxes and to conclude about their primary function depending on chemical composition. Fluxes SF1, SF2, and SF3 can be referred to as covering-refining fluxes because, in addition to the prevailing

refining components (simple and double chlorides of K and Mg), they contain up to 15% NaCl and up to 25% KCl, which give the mixture covering properties, promoting uniform distribution on the surface of the melt. Whereas fluxes SF4 and SF5 can be characterized strictly as refining fluxes. It should be noted that the main components of the mixtures under discussion are chlorides (single, binary, hydrated), which, in conjunction with the hygroscopicity of additives, imply careful observance of storage conditions and heating before use.

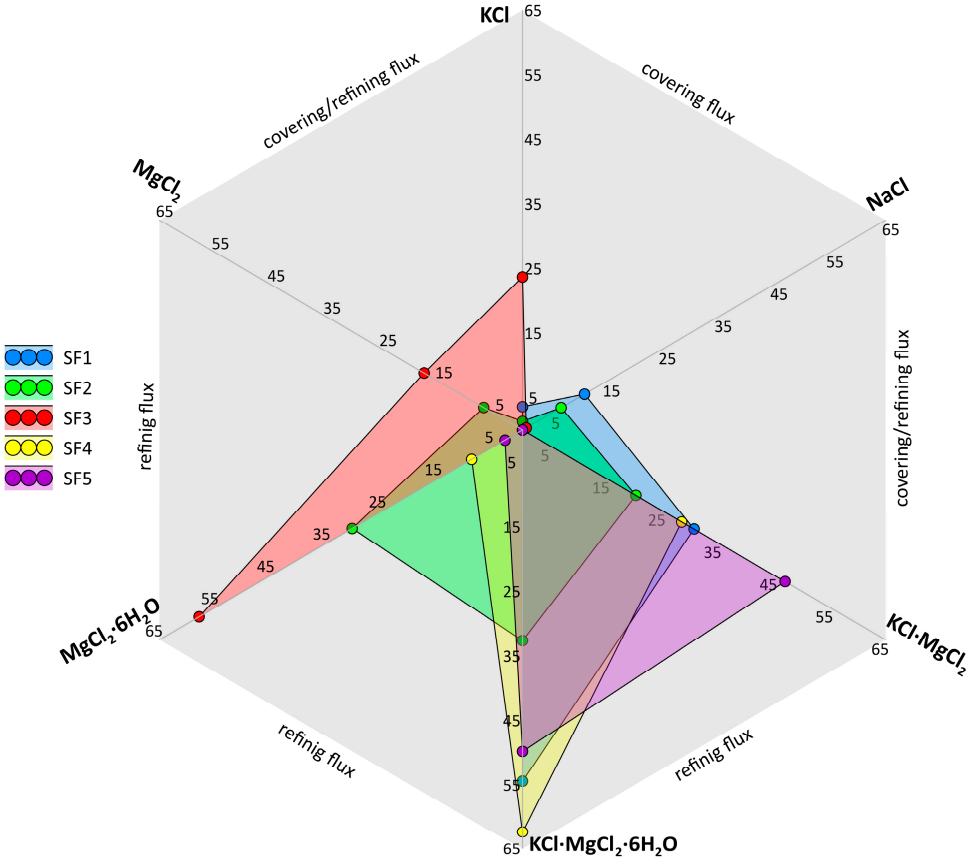

Figure 6. Phase composition diagram of the investigated salt fluxes (wt.%). Only the axes of the main functional components are shown.

By converting the identified compositions to the dehydrated state, it is also possible to calculate their density in the liquid state according to the principle of additivity based on the known data on the properties of the individual components [62–64], as shown in Table 4. The density difference between the melt and liquid salt fluxes ranges from 0.737 to 0.832 g/cm^3, which is a satisfactory value for their successful separation.

Table 4. Flux chemical compositions and densities.

Flux	Calculated Composition in Dehydrated State (wt.%)					Calculated Liquid Density (g/cm^3)	Molten Alloy Density (g/cm^3)
	KCl	NaCl	$MgCl_2$	$KCl{\cdot}MgCl_2$	CaF_2		
SF1	4.580	14.12	–	81.30	–	1.568	2.400
SF2	1.860	9.740	29.91	56.74	1.750	1.663	
SF3	34.30	0.940	64.76	–	–	1.626	
SF4	–	–	6.000	94.00	–	1.652	
SF5	–	–	1.900	98.10	–	1.651	

3.2. Moisture Content

As can be seen from the analysis of the chemical composition, almost all the studied salt fluxes contain crystalline hydrates, which directly indicates the presence of hygroscopic and crystallization moisture. Additional saturation of fluxes with moisture in contact with the atmosphere of the warehouse or foundry during the production process will inevitably have a negative impact when loading materials into metallurgical aggregates. This will contribute to increased hydrogen concentrations in the aluminum melt, especially if flux storage and use regulations are not followed. Explosive heating of such flux when introduced into the molten metal will lead to the decomposition of crystalline hydrates with the release of water vapor, which not only enters the atmosphere of the aggregate but also partially reacts with aluminum according to Equation (1), saturating it with hydrogen and contributing to the formation of inclusions [62]. It is also possible that water vapor will interact with magnesium, potassium, and sodium chlorides, which will cause the emission of hydrogen chloride.

$$2Al + 3H_2O = Al_2O_3 + 6H \quad (1)$$

Figure 7 shows thermograms of the studied salt fluxes. The blue line of the differential thermal analysis (DTA) characterizes the thermal effects during the heating of the sample; the green line is the thermogravimetric (TG) curve showing the weight changes of the sample. The character of the SF1 thermogram (Figure 7a) is identical to the process of dehydration of double chloride $KCl{\cdot}MgCl_2{\cdot}6H_2O$ at atmospheric pressure in air, which proceeds in two stages. First, the hexahydrate decomposes to the dihydrate ($KCl{\cdot}MgCl_2{\cdot}2H_2O$). This transformation starts at 105 °C and ends around 155 °C with the transition to the second stage of dehydration. The second stage consists of dehydration of the dihydrate to an anhydrous compound ($KCl{\cdot}MgCl_2$) and is completed at 230 °C (endo-effect with a maximum at 180.40 °C). The total release of hygroscopic and crystallization moisture when heating the SF1 flux to 300 °C was about 6.7%.

For the SF2 sample on the DTA line, the endothermic effect associated with the onset of water release from the sample is observed below 100 °C (Figure 7b). The endothermic effects at 129.14 °C and 181.32°C and their corresponding weight loss of flux are due to the decomposition of $KCl{\cdot}MgCl_2{\cdot}6H_2O$. The endothermic effects of dehydration in this case are superimposed on the effects of the decomposition of the second crystalline hydrate, $MgCl_2{\cdot}6H_2O$. Dehydration occurs in steps, with two water molecules each released at 117 °C, 185 °C, and 246.58 °C, respectively. The endo-effect at 382.53 °C is associated with the onset of flux melting. The total amount of moisture released from the SF2 flux when heating to 300 °C amounted to 9.6%.

The endothermic deviation of the DTA line for SF3, associated with the release of hygroscopic moisture from the sample, is also observed below 100 °C (Figure 7c). The endothermic effects at 126.81 °C, 178.45°C, and 254.18 °C and their corresponding weight loss of flux are due to the decomposition of $MgCl_2{\cdot}6H_2O$ crystalline hydrates with the loss of two water molecules at each endothermic effect. The weight loss of the sample at 126.81 °C was 1.7%, 2.8% at 178.45 °C, and 4.3% at 254.18 °C. Presumably, the uneven weight loss during the stage of dehydration of magnesium chloride is due to diffusion difficulties in the release of moisture during the decomposition of crystalline hydrate. Dehydration of SF3 flux components includes two sequential-parallel processes: decomposition of crystalline hydrates with separation of several water molecules and desorption of water released from crystalline hydrates. These processes proceed at different rates, which are determined by the conditions of sample taking. It is obvious that desorption of moisture from crystalline hydrate was somewhat "delayed" relative to the thermal effects of dissociation. The total amount of moisture released from the SF3 flux during heating to 270 °C was 8.8%. Further

heating of the flux up to 380 °C is accompanied by the release of gaseous HCl in the amount of 0.8%.

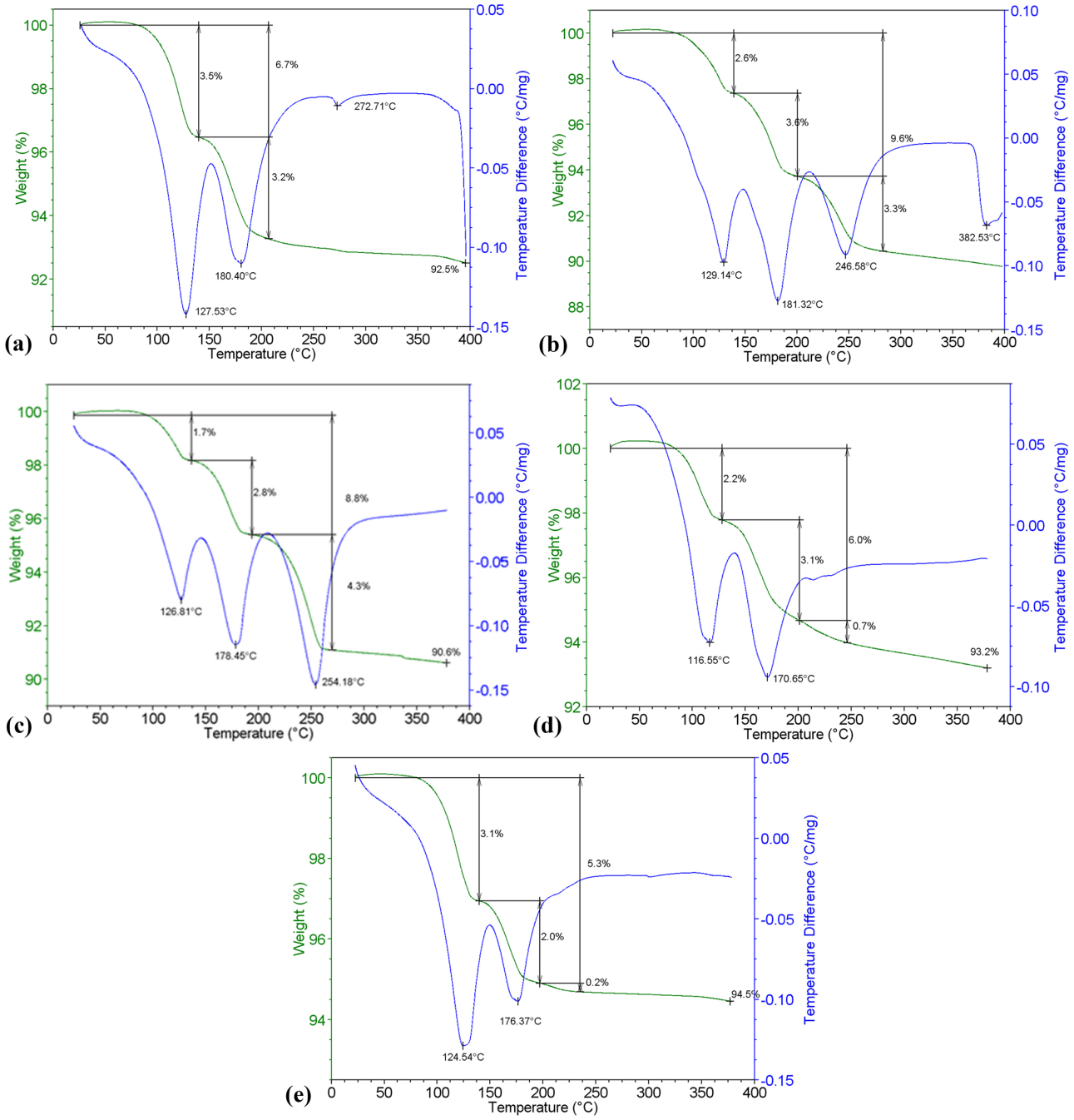

Figure 7. Thermograms of the investigated salt fluxes: (**a**) SF1; (**b**) SF2; (**c**) SF3; (**d**) SF4; (**e**) SF5.

The moisture in the SF4 flux is also represented by the crystalline hydrates $KCl{\cdot}MgCl_2{\cdot}6H_2O$ and $MgCl_2{\cdot}6H_2O$. The endothermic effects at 116.55 °C and 170.65 °C and their corresponding weight loss are primarily due to the decomposition of $KCl{\cdot}MgCl_2{\cdot}6H_2O$ (Figure 7d). As in the case of the SF2 flux, the effects of $MgCl_2{\cdot}6H_2O$ decomposition are superimposed on the endo effects of the dehydration of the double chloride. In this case, the effects of dehydration of the more complex compound dominate, since its concentration in the sample is much higher than the content of simple magnesium chloride. The weight loss of the sample at 116.55 °C was 2.2%; further at 170.65°C, another 3.1%. The total amount of moisture released during heating to a temperature of 250 °C was 6.0%.

The presence of crystallization moisture in the SF5 flux is confirmed by the character of DTA and TG curves on the thermogram (Figure 7e). The endothermic effects on the DTA line at 124.54 °C and 176.37°C and their corresponding weight loss are caused by the decomposition of $KCl{\cdot}MgCl_2{\cdot}6H_2O$ crystalline hydrate. The first stage of dehydration corresponds to the endothermic effect at 124.54 °C with a weight loss of 3.1%. In the second stage at 176.37 °C, the double chloride loses the two remaining water molecules with a weight loss of another 2.0%. The dehydration effects of $MgCl_2{\cdot}6H_2O$ are not recognized because they are superimposed on the effects of $KCl{\cdot}MgCl_2{\cdot}6H_2O$ decomposition. This is due to the concentration features of the composition of this flux (see Table 4). The total amount of moisture released from SF5 during heating to 240 °C was 5.3%.

3.3. Melting Temperature

The state diagrams of the salt systems used as components to design fluxes are mostly of the eutectic type, and the melting point is in a wide range from 288 to 945 °C [57,67]. The melting point plays an important role in the effective performance of the salt flux. Relatively high-melting-point compositions, when saturated with slag inclusions, rapidly thicken and harden. As a result, the amount of slag removed decreases and metal losses increase. For effective flux treatment of aluminum melt, it is necessary that the melting temperature of the flux be lower than the temperature of the processed metal.

On the one hand, the melting point can be determined theoretically for the basic flux components using the state diagrams of the systems NaCl–KCl–$MgCl_2$ and KCl–$MgCl_2$ [67,68], while it is necessary to recalculate the identified compositions to the anhydrous state of single chlorides. As an example, consider the flux SF1: to find the position of the composition point of the investigated flux on the ternary diagram, it is necessary to draw straight lines parallel to the sides of the triangle and corresponding to the concentrations of each compound, as shown in Figure 8. At the intersection of the three lines (highlighted in red) is the figurative point of the flux composition. This point for SF1 corresponds to a melting point of about 410 °C.

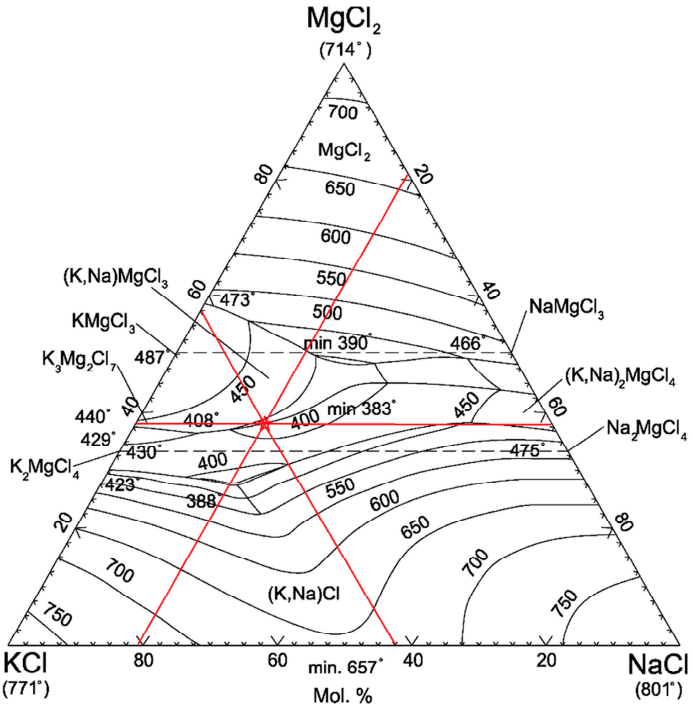

Figure 8. Position of the SF1 flux point on the state diagram of the NaCl–KCl–$MgCl_2$ system. The ternary diagram is reprinted with permission from Ref. [67]. 2012 Pyrotek, Inc.

On the other hand, when performing the experiment according to the method [60] described above, it is possible to obtain data directly on the melting ranges of the compositions under consideration and the mass loss of the samples that occurs during this process. The comparative results of both methods are shown in Figure 9. Thus, all the compositions can be considered as easily melting, since their melting point is on average 200–250 °C lower than that of the molten metal in the metallurgical unit. At the same time, the relatively low weight loss of the samples (no more than 2.4%) suggests that, firstly, the fluxes were not completely freed from their own crystallization moisture; secondly, they melted and dissolved into it.

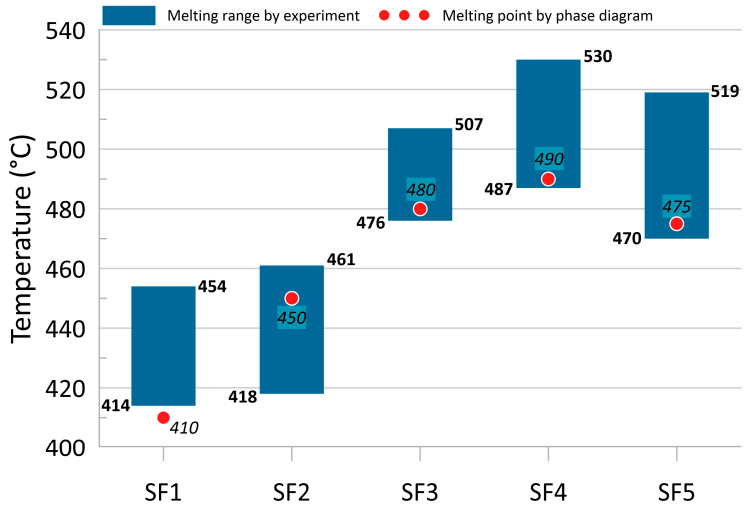

Figure 9. Measured melting ranges and calculated melting points of the investigated fluxes.

3.4. Particle Size Distribution

In a comparative analysis of the particle size distribution shown in Figure 10, three fluxes should be distinguished—SF2, SF4, and SF5. These three compositions are characterized by the maximum content of particles larger than 0.5 mm and practically do not contain a dust-like fraction. The uniform and coarse particle size distribution of the above compositions has a positive effect on their operational properties: first of all, it concerns mechanical losses of flux, as well as losses due to evaporation and pyrohydrolysis.

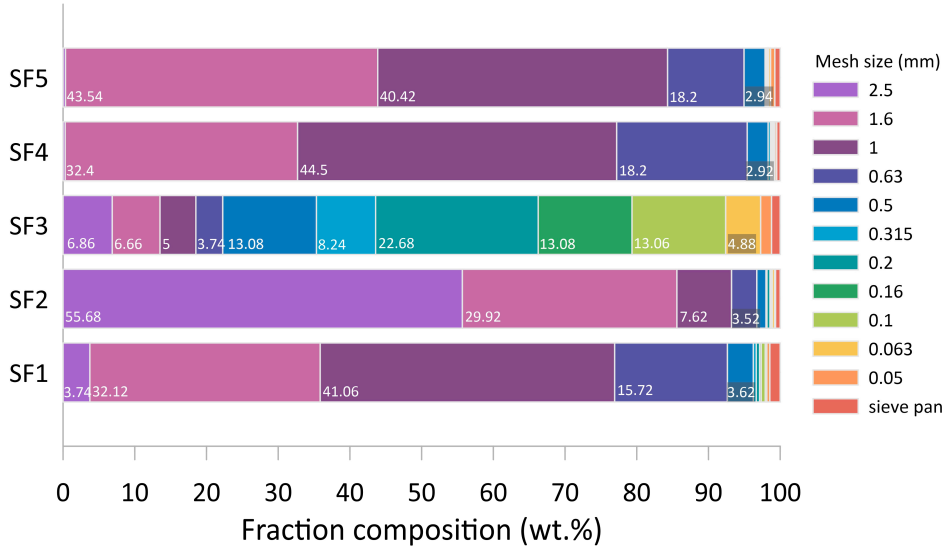

Figure 10. Material distribution of the investigated fluxes on the calibrator meshes.

From this point of view, flux SF1 is slightly inferior due to an almost 2 times higher content of dust-like fraction. The most non-uniform composition possesses flux SF3: 65% of the weight of the sample falls on the fine and dust-like fraction (0.315 mm and smaller). The non-uniform and finely dispersed structure promotes the bringing of particles of flux by streams of hot air under a dome of the foundry unit and settling on heaters, reducing their service life.

3.5. Melt Refining Efficiency

The efficiency of all five salt fluxes was evaluated on aluminum-magnesium alloy doped with scandium (see Table 2) by the change of Na, Ca, and H_2 content before and after treatment. The initial content of Ca, Na, and H_2 in the state before fluxing corresponds to the average values in the real production process, formed as a combination of contamination of charge materials and alloying components, deviations in their declared chemical composition, presence of traces of lubricants on their surface, as well as humidity in the shop atmosphere or on the tool surface. The comparative results of this experiment are summarized in Table 5. In this case, the mechanism of aluminum alloy refining is based on exchange reactions between sodium and calcium compounds and chlorides contained in fluxes, as well as aluminum chloride formed as a result of the interaction of metal with hydrogen chloride.

Table 5. Experimental results of melt treatment using investigated fluxes.

Flux	Na (ppm)		Ca (ppm)		H_2 (cm^3/100 g)	
	Before	After	Before	After	Before	After
SF1	2.30	<1.00	3.00	<1.00	0.20	0.16
SF2	4.10	3.10	13.0	2.70	0.27	0.22
SF3	9.00	1.00	50.0	<1.00	0.25	0.13
SF4	55.0	<1.00	1.60	1.20	0.22	0.13
SF5	28.0	1.90	24.0	2.10	0.21	0.18

To explain possible interactions in the system of aluminum-flux melts, it is possible to follow the electrochemical activity series of metals: standard electrode potentials of metals that can participate in exchange reactions K^+ (−2.92); Ca^{2+} (−2.87); Na^+ (−2.71); Mg^{2+} (−2.36); Al^{3+} (−1.66) [64]. Obviously, of the three chlorides contained in fluxes (KCl, NaCl, and $MgCl_2$), only $MgCl_2$ can participate in exchange reactions for chlorination of sodium and calcium impurities, since the Mg^{2+} ion is more electropositive than Na^+ and Ca^{2+} ions. The main interactions of impurities with $MgCl_2$ can be presented in the form of Equations (2) and (3):

$$MgCl_2 + 2Na = 2NaCl + Mg \quad (2)$$

$$MgCl_2 + Ca = CaCl_2 + Mg \quad (3)$$

Synthesis of aluminum chloride is possible by interaction of aluminum with gaseous HCl, a product of hydrolysis of $MgCl_2$. Subsequent possible reactions of $AlCl_3$ with Na and Ca impurities are described by Equations (4) and (5):

$$AlCl_3 + 3Na = 3NaCl + Al \quad (4)$$

$$2AlCl_3 + 3Ca = 3CaCl_2 + 2Al \quad (5)$$

Degassing of metal during fluxing is carried out by two mechanisms. Firstly, part of the hydrogen is removed in adsorbed form together with dross inclusions. Secondly,

dissolved hydrogen is removed from the melt in the form of HCl as a result of exchange reactions with magnesium and aluminum chlorides according to Equations (6) and (7):

$$MgCl_2 + H_2 = Mg + 2HCl\uparrow \quad (6)$$

$$AlCl_3 + 1.5H_2 = Al + 3HCl\uparrow \quad (7)$$

As it was shown in previously published papers [24,31,60], in order to reduce the dissolved hydrogen content during melt treatment with fluxes containing crystalline hydrates of various chlorides, it is necessary, first of all, to ensure proper storage of materials, their preheating and drying, or to switch to the application of fused refining and covering-refining fluxes, which will also avoid the dust-like fraction being entrained into the atmosphere of the foundry site. Otherwise, fluxes containing hygroscopic and crystallization moisture do not refine the melt but additionally saturate it with hydrogen, causing the formation of inclusions and subsequent defects in the products.

4. Conclusions

This paper presents a comprehensive study of five commercial solid salt fluxes (conventionally designated SF1, SF2, SF3, SF4, and SF5) to better understand the relationship between composition, properties, and melt refining efficiency. The study was realized through the combination of standard analytical methods and a number of experiments close to the conditions of industrial direct chill casting. Based on the reported results, the following conclusions can be drawn:

- The obtained XRD patterns give a clear picture of the composition of the studied mixtures, the main components of which are simple and double chlorides of potassium, sodium, and magnesium. According to known functions of separate components, it is established that fluxes SF1, SF2, and SF3 are covering and refining, and fluxes SF4 and SF5 are only refining;
- The fluxes under consideration contain hygroscopic and crystallization moisture and can melt and dissolve in it under heating. For flux SF1, the moisture content was 6.7%; for SF2, 9.6%; for SF3, 8.8%; for SF4, 6%; and for SF5, 5.3%;
- The main sources of moisture are crystalline hydrates $KCl{\cdot}MgCl_2{\cdot}6H_2O$ and $MgCl_2{\cdot}6H2O$ contained in the fluxes in an amount ranging from 3 to 62%;
- The studied fluxes are easy to melt because the calculated melting point (less than 550 °C) and practically measured melting range (less than 530 °C) allow the slag to remain liquid even at significant saturation with oxide inclusions;
- The fluxes SF2, SF4, and SF5 have a uniform fractional distribution with predominantly coarse particles (97% larger than 0.5 mm) and are suitable for industrial applications, whereas the high proportion of fine fractions in SF1 and SF3 (around 90% larger than 0.5 mm) makes them prone to losses during storage and operation;
- According to decreasing refining efficiency, the investigated compositions can be arranged in the following order: SF3, SF4, SF5, SF2, and SF1, which agrees with the known data on the performance of fluxes based on KCl and $MgCl_2$ as applied to Al—Mg alloys.

Significantly, the negative effect of moisture in salt fluxes is not only in the saturation of aluminum melt with hydrogen and its oxidation: if a batch of material in the amount of 10 tons is purchased, the consumer also pays for 0.5 to 1.0 tons of hygroscopic and crystallization water. When using the considered salt fluxes, taking into account their low melting point and tendency to evaporate and hydrolyze, it is recommended to maintain the temperature of the processed melt at about 690–730 °C.

Author Contributions: Conceptualization, B.K. and Y.M.; methodology, B.K.; validation, E.P., A.K. and N.S.; formal analysis, B.K., E.P., A.K., Y.B. and D.B.; investigation, E.P., A.K., N.S., Y.B., D.B., A.D., N.D. and M.B.; resources, P.Y., A.D., N.D. and M.B.; data curation, B.K., E.P., P.Y., N.D. and M.B.; writing—original draft preparation, A.K.; writing—review and editing, A.K. and E.P.; visualization, A.K. and N.D.; supervision, B.K. and Y.M.; project administration, P.Y. and N.S. All authors have read and agreed to the published version of the manuscript.

Funding: This research received no external funding.

Data Availability Statement: The data presented in this study are available on reasonable request from the corresponding author. The data are not publicly available due to privacy.

Conflicts of Interest: The authors declare no conflicts of interest.

References

1. Lehmhus, D. Advances in Metal Casting Technology: A Review of State of the Art, Challenges and Trends—Part I: Changing Markets, Changing Products. *Metals* **2022**, *12*, 1959. [CrossRef]
2. Raabe, D.; Ponge, D.; Uggowitzer, P.J.; Roscher, M.; Paolantonio, M.; Liu, C.; Antrekowitsch, H.; Kozeschnik, E.; Seidmann, D.; Gault, B.; et al. Making sustainable aluminum by recycling scrap: The science of "dirty" alloys. *Prog. Mater. Sci.* **2022**, *128*, 100947. [CrossRef]
3. Statistics—International Aluminium Institute. Available online: https://international-aluminium.org/statistics-overview/ (accessed on 18 March 2025).
4. Uzyakov, M.N.; Kolpakov, A.Y.; Porfiriev, B.N.; Galinger, A.A.; Yantovskii, A.A. Materials and energy intensity of the global carbon neutrality. *Stud. Russ. Econ. Dev.* **2023**, *34*, 335–341. [CrossRef]
5. Billy, R.G.; Müller, D.B. Aluminium use in passenger cars poses systemic challenges for recycling and GHG emissions. *Resour. Conserv. Recycl.* **2022**, *190*, 106827. [CrossRef]
6. Li, S.; Yue, X.; Li, Q.; Peng, H.; Dong, B.; Liu, T.; Yang, H.; Fan, J.; Shu, S.; Qiu, F.; et al. Development and applications of aluminum alloys for aerospace industry. *J. Mater. Res. Technol.* **2023**, *27*, 944–983. [CrossRef]
7. Reva, D.; Lisyatnikov, M.; Prusov, E. Mechanical behavior of aluminum matrix composites in the elements of building structures. In Proceedings of the International Conference on Materials Physics, Building Structures and Technologies in Construction, Industrial and Production Engineering (MPCPE), Vladimir, Russia, 26–28 April 2022; pp. 323–331. [CrossRef]
8. Liu, S.; Zhao, T.; Fu, J.; Zu, Q. Development of Inoculants for Aluminum Alloy: A Review. *Materials* **2023**, *16*, 5500. [CrossRef]
9. Arowosola, A.; Gaustad, G. Estimating increasing diversity and dissipative loss of critical metals in the aluminum automotive sector. *Resour. Conserv. Recycl.* **2019**, *150*, 104382. [CrossRef]
10. Wang, B.; Zhang, Z.; Xu, G.; Zeng, X.; Hu, W.; Matsubae, K. Wrought and cast aluminum flows in China in the context of electric vehicle diffusion and automotive lightweighting. *Resour. Conserv. Recycl.* **2023**, *191*, 106877. [CrossRef]
11. Lütkehaus, H.; Pade, C.; Oswald, M.; Brand, U.; Naegler, T.; Vogt, T. Measuring raw-material criticality of product systems through an economic product importance indicator: A case study of battery-electric vehicles. *Int. J. Life Cycle Assess.* **2021**, *27*, 122–137. [CrossRef]
12. Torta, G.; Ciacci, L.; Vassura, I.; Passarini, F. Exploring mass and economic potentials of rare earth elements recycling from electric vehicles at end-of-life. *Miner. Econ.* **2024**, *37*, 573–587. [CrossRef]
13. Alamdari, H. Aluminium production process: Challenges and opportunities. *Metals* **2017**, *7*, 133. [CrossRef]
14. Curtolo, D.C.; Xiong, N.; Friedrich, S.; Friedrich, B. High- and Ultra-High-Purity Aluminum, A review on technical production methodologies. *Metals* **2021**, *11*, 1407. [CrossRef]
15. Nunes, H.; Emadinia, O.; Soares, R.; Vieira, M.F.; Reis, A. Adding Value to Secondary Aluminum Casting Alloys: A review on Trends and Achievements. *Materials* **2023**, *16*, 895. [CrossRef]
16. Penya, A.F.; Bazhin, V.Y.; Makushin, D.V. Valuable aluminum alloys obtained from secondary metallized raw materials. *iPolytech J.* **2025**, *28*, 647–656. [CrossRef]
17. Capuzzi, S.; Timelli, G. Preparation and melting of scrap in Aluminum Recycling: A review. *Metals* **2018**, *8*, 249. [CrossRef]
18. Nikitin, V.I.; Nikitin, K.V.; Timoshkin, I.Y.; Biktimirov, R.M. Synthesis of Aluminum Alloys from Dispersed Waste Based on Aluminum. *Russ. J. Non-Ferr. Met.* **2020**, *61*, 632–640. [CrossRef]
19. Kawajiri, K.; Kobayashi, M.; Sakamoto, K. Lightweight materials equal lightweight greenhouse gas emissions?: A historical analysis of greenhouse gases of vehicle material substitution. *J. Clean. Prod.* **2019**, *253*, 119805. [CrossRef]
20. Campbell, J.; Tiryakioğlu, M. Fatigue Failure in Engineered Components and How It Can Be Eliminated: Case Studies on the Influence of Bifilms. *Metals* **2022**, *12*, 1320. [CrossRef]

21. Campbell, J. *The Mechanisms of Metallurgical Failure*; Butterworth–Heinemann: Oxford, UK, 2020; ISBN 978-0-12-822411-3. [CrossRef]
22. Wu, J.; Djavanroodi, F.; Gode, C.; Attarilar, S.; Ebrahimi, M. Melt refining and purification processes in Al alloys: A comprehensive study. *Mater. Res. Express* **2022**, *9*, 032001. [CrossRef]
23. Lazaro-Nebreda, J.; Patel, J.B.; Lordan, E.; Zhang, Y.; Karakulak, E.; Al-Helal, K.; Scamans, G.M.; Fan, Z. Degassing of aluminum alloy melts by high shear melt conditioning technology: An overview. *Metals* **2022**, *12*, 1772. [CrossRef]
24. Belyaev, S.V.; Partyko, E.G.; Kosovich, A.A.; Baranov, V.N.; Bezrukikh, A.I.; Gubanov, I.Y.; Gorokhov, Y.V.; Koptseva, N.P.; Kirko, V.I.; Lesiv, E.M.; et al. Analysis of plain aluminium saturation with hydrogen while adding different components. *ARPN J. Eng. Appl. Sci.* **2018**, *13*, 3251–3256.
25. Gómez, E.R.; Zenit, R.; Rivera, C.G.; Trápaga, G.; Ramírez-Argáez, M.A. Physical Modeling of Fluid Flow in Ladles of Aluminum Equipped with Impeller and Gas Purging for Degassing. *Metall. Mater. Trans. B* **2013**, *44*, 974–983. [CrossRef]
26. Mastrullo, R.; Mauro, A.W.; Pelella, F.; Viscito, L. Process control and energy saving in the ladle stage of a metal casting process through physics-based and ANN-based modelling approaches. *Appl. Therm. Eng.* **2024**, *248*, 123135. [CrossRef]
27. Abramov, V.O.; Abramova, A.V.; Bayazitov, V.M.; Nikonov, R.V.; Cravotto, G. Pores-free aluminium alloy by efficient degassing ultrasonic treatments. *Appl. Acoust.* **2021**, *184*, 108343. [CrossRef]
28. Liu, G.; Ren, Y.; Ma, W.; Morita, K.; Lei, Y.; Zhan, S.; Lv, G.; Li, S.; Wang, Z.; Li, R. Recent advances and future trend of aluminum alloy melt purification: A review. *J. Mater. Res. Technol.* **2024**, *28*, 4647–4662. [CrossRef]
29. Deev, V.B.; Prusov, E.S.; Kutsenko, A.I. Theoretical and experimental evaluation of the effectiveness of aluminum melt treatment by physical methods. *Metall. Ital.* **2018**, *110*, 16–24.
30. Martínez-Pañeda, E.; Niordson, C.F.; Gangloff, R.P. Strain gradient plasticity-based modeling of hydrogen environment assisted cracking. *Acta Mater.* **2016**, *117*, 321–332. [CrossRef]
31. Baranov, V.N.; Kulikov, B.P.; Partyko, E.G.; Kosovich, A.A. Effect of alloying, modifying and fluxing agents on aluminum hydrogen saturation. *Tsvetnye Met.* **2021**, *7*, 45–51. [CrossRef]
32. Puga, H.; Barbosa, J.; Carneiro, V.H.; Barbosa, F.V.; Teixeira, J.C. Optimizing high-volume ultrasonic melt degassing using synchronized kinematic translation. *J. Mater. Res. Technol.* **2021**, *14*, 2832–2844. [CrossRef]
33. Piękoś, M.; Smorawiński, Z. Introduction of powder fluxes in rotary degassing system towards intensifying refining process of aluminium alloys. *Arch. Foundry Eng.* **2024**, *24*, 89. [CrossRef]
34. Ren, Y.; Chen, H.; Ma, W.; Lei, Y.; Zeng, Y. Purification of aluminium-silicon alloy by electromagnetic directional solidification: Degassing and grain refinement. *Sep. Purif. Technol.* **2021**, *277*, 119459. [CrossRef]
35. Lu, G.-H.; Zhang, Y.; Deng, S.; Wang, T.; Kohyama, M.; Yamamoto, R.; Liu, F.; Horikawa, K.; Kanno, M. Origin of intergranular embrittlement of Al alloys induced by Na and Ca segregation: Grain boundary weakening. *Phys. Rev. B* **2006**, *73*, 224115. [CrossRef]
36. Görner, H.; Engh, T.A.; Syvertsen, M.; Zhang, L.F. Removal of Na and Ca from Aluminum Scrap through Filtration. *Mater. Sci. Forum* **2007**, *546–549*, 801–806. [CrossRef]
37. Glazoff, M.V.; Zolotorevsky, V.S.; Belov, N.A. *Casting Aluminum Alloys*; Elsevier Science Pub Co.: Amsterdam, The Netherlands, 2007; ISBN 978-0-08-045370-5. [CrossRef]
38. Williams, E.M.; McCarthy, R.W.; Levy, S.A.; Sigworth, G.K. Removal of Alkali Metals from Aluminum. In *Essential Readings in Light Metals*; Grandfield, J.F., Eskin, D.G., Eds.; Springer: Cham, Switzerland, 2016; pp. 71–79. ISBN 978-3-319-48576-8. [CrossRef]
39. Wang, H.; Fu, G.; Cheng, C.; Wang, L. Highly Efficient and Environmental Process for Removing Alkali Metals from Aluminum Melt. *Met. Sci. Heat Treat.* **2019**, *61*, 90–95. [CrossRef]
40. Huang, C.; Liu, Z.; Huang, J.; Liu, Q.; Li, J. Effect of Sodium-Containing fluxes on the residual sodium content and distribution in Al–Mg alloys. *Metals* **2021**, *11*, 1591. [CrossRef]
41. Belov, N.A.; Aksenov, A.A.; Eskin, D.G. *Iron in Aluminium Alloys*; CRC Press: London, UK, 2002; ISBN 978-0415273527. [CrossRef]
42. Zhang, L.; Damoah, L.N. Current Technologies for the Removal of Iron from Aluminum Alloys. In *Essential Readings in Light Metals*; Grandfield, J.F., Eskin, D.G., Eds.; Springer: Cham, Switzerland, 2016; pp. 101–106. ISBN 978-3-319-48576-8. [CrossRef]
43. Zhang, Y.-B.; Kateryna, S.; Li, T.-J. Effect of ultrasonic treatment on formation of iron-containing intermetallic compounds in Al-Si alloys. *China Foundry* **2016**, *13*, 316–321. [CrossRef]
44. Sun, Y.; Huang, X.; Liu, C.; Zhou, M.; Zhang, X. Impurity iron separation from molten secondary aluminum by pulsed electric current. *J. Alloys Compd.* **2022**, *934*, 167903. [CrossRef]
45. Sanchez, J.M.; Arribas, M.; Galarraga, H.; De Cortazar, M.G.; Ellero, M.; Girot, F. Effects of Mn addittion, cooling rate and holding temperature on the modification and purification of iron-rich compounds in AlSi10MnMg(Fe) alloy. *Heliyon* **2023**, *9*, e13005. [CrossRef]
46. Li, C.; Li, J.-G.; Mao, Y.-Z.; Ji, J.-C. Mechanism to remove oxide inclusions from molten aluminum by solid fluxes refining method. *China Foundry* **2017**, *14*, 233–243. [CrossRef]

47. Voigt, C.; Hubálková, J.; Bergin, A.; Fritzsch, R.; Aune, R.; Aneziris, C.G. Overview of the possibilities and limitations of the characterization of ceramic foam filters for metal melt filtration. In *Light Metals 2021*; Perander, L., Ed.; Springer: Cham, Switzerland, 2021; pp. 785–793. ISBN 978-3-030-65395-8. [CrossRef]
48. Li, Y.; Wang, C.; Mi, G. Influence of cleaning modes on the microstructure and performance of 5083 alloy substrate. *J. Mech. Sci. Technol.* **2021**, *35*, 3943–3949. [CrossRef]
49. Gyarmati, G.; Vincze, F.; Fegyverneki, G.; Kéri, Z.; Mende, T.; Molnár, D. The Effect of Rotary Degassing Treatments with Different Purging Gases on the Double Oxide- and Nitride Film Content of Liquid Aluminum Alloys. *Metall. Mater. Trans. B* **2022**, *53*, 1244–1257. [CrossRef]
50. Dai, Y.; Voigt, C.; Storti, E.; Hubálková, J.; Gehre, P.; Liang, X.; Yan, W.; Li, Y.; Aneziris, C.G. Open-cell ceramic foam filters for melt filtration: Processing, characterization, improvement and application. *J. Mater. Res. Technol.* **2024**, *32*, 3402–3422. [CrossRef]
51. Liu, C.; Hu, Z.L.; Zeng, J.M. Removal of impurities in aluminum by uses of fluxes. *Adv. Mat. Res.* **2012**, *509*, 152–155. [CrossRef]
52. Utigard, T.A.; Roy, R.R.; Friesen, K. The roles of molten salts in the treatment of aluminum. *Can. Metall. Quart.* **2001**, *40*, 327–334. [CrossRef]
53. Tenorio, J.A.S.; Carboni, M.C.; Espinosa, D.C.R. Recycling of aluminum–effect of fluoride additions on the salt viscosity and on the alumina dissolution. *J. Light Met.* **2001**, *1*, 195–198. [CrossRef]
54. Shi, M.; Li, Y. Performance Improvement in Aluminum Alloy Treated by Salt Flux with Different Fluorides. *J. Mater. Eng. Perform.* **2022**, *32*, 3065–3072. [CrossRef]
55. Milani, V.; Timelli, G. Solid salt fluxes for Molten Aluminum Processing—A review. *Metals* **2023**, *13*, 832. [CrossRef]
56. Wan, B.; Li, W.; Liu, F.; Lu, T.; Jin, S.; Wang, K.; Yi, A.; Tian, J.; Chen, W. Determination of fluoride component in the multifunctional refining flux used for recycling aluminum scrap. *J. Mater. Res. Technol.* **2020**, *9*, 3447–3459. [CrossRef]
57. Zhang, G.; Lu, W.; Wu, X.; Yang, B.; Tan, Y.; Xu, Z.; Tang, H.; Zeng, J.; Wang, J. A new strategy on designing fluxes for aluminum alloy melt refinement. *Materials* **2023**, *16*, 2322. [CrossRef]
58. Aydogan, F.; Dizdar, K.C.; Sahin, H.; Mentese, E.; Dispinar, D. Mechanical property comparison of AL11Si wheels grain refined by Ti, Nb and MTS. *Arch. Foundry Eng.* **2022**, *22*, 14–18. [CrossRef]
59. Aydogan, F.; Dizdar, K.C.; Sahin, H.; Mentese, E.; Dispinar, D. Weibull analysis evaluation of Ti, B, Nb and MTS grain refined Al11Si alloy. *Mater. Chem. Phys.* **2022**, *287*, 126264. [CrossRef]
60. Kulikov, B.P.; Baranov, V.N.; Partyko, E.G.; Kostin, I.V.; Yur'ev, P.O.; Yanov, V.V. Comparative Studies into Composition and Properties of FPR-23 and Biomag Covering and Degassing Fluxes. *Metallurgist* **2022**, *66*, 290–298. [CrossRef]
61. Bogdanova, T.A.; Merkulova, G.A.; Gilmanshina, T.R.; Kosovich, A.A.; Lytkina, S.I.; Cheglakov, A.V.; Antonov, M.M. Comparative evaluation of methods for determination of hydrogen and non-metallic inclusions content in aluminum alloys. *ARPN J. Eng. Appl. Sci.* **2021**, *16*, 355–360.
62. Utigard, T.A. The properties and uses of fluxes in molten aluminum processing. *JOM* **1998**, *50*, 38–43. [CrossRef]
63. Janz, G.J. Thermodynamic and Transport Properties for Molten Salts: Correlated Equations for Critically Evaluated Density, Surface Tension, Electrical Conductance, and Viscosity Data. *J. Phys. Chem. Ref. Data* **1988**, *17*, 311.
64. Law, J.; Rennie, R. (Eds.) *A Dictionary of Chemistry*, 8th ed.; Oxford University Press: Oxford, UK, 2020; ISBN 9780198841227. [CrossRef]
65. Teterin, V.; Mikhajlov, E.; Shundikov, N.; Arteev, A.; Elin, S.; Bezdolja, I. Method of Flux Production for Melting and Refining of Magnesium or Its Alloys. RU Patent 2492252, 10 September 2013.
66. Frolov, V.; Zajtsev, A.; Kulikov, B. Halogen-Containing Flux Preparation Method for the Aluminium and Its Alloys Processing. RU Patent 2657680, 14 June 2018.
67. Tremblay, S.; Desrosiers, L.; Levesque, D. Use of a Tertiary Salt Flux of NaCl, KCl, and $MgCl_2$ for the Purification of Aluminium or Aluminium Alloys, and Method Thereof. U.S. Patent 2012/0017726, 26 January 2012.
68. Villada, C.; Ding, W.; Bonk, A.; Bauer, T. Engineering molten $MgCl_2$–KCl–NaCl salt for high-temperature thermal energy storage: Review on salt properties and corrosion control strategies. *Sol. Energ. Mat. Sol. Cells* **2021**, *232*, 111344. [CrossRef]

Disclaimer/Publisher's Note: The statements, opinions and data contained in all publications are solely those of the individual author(s) and contributor(s) and not of MDPI and/or the editor(s). MDPI and/or the editor(s) disclaim responsibility for any injury to people or property resulting from any ideas, methods, instructions or products referred to in the content.